

A CLASS OF ELECTRO-MECHANICAL SYSTEMS: LINEAR AND NONLINEAR DYNAMICS

FRANCESCO DELL'ISOLA
FABRIZIO VESTRONI
STEFANO VIDOLI

Dipartimento Ingegneria Strutturale e Geotecnica, Università degli Studi di Roma "La Sapienza"
e-mail: francesco.dellisola@uniroma1.it

The linear and nonlinear problems of dynamics of some electro-mechanical systems, characterized by a gyroscopic internal coupling, are analyzed. Since the technical importance of this system lies in the possibility of damping and controlling structural vibrations, the interest is focused on the energy exchanges between the mechanical and electric components. In order to maximize these energy transformations, the optimal values of the system parameters and their modifications in the nonlinear case are investigated.

Key words: electro-mechanical system, energy transformation, structural vibration

1. Introduction

Different kind of electromechanical coupling phenomena has been used in engineering applications. An exhaustive and detailed discussion of the foundations of this part of engineering science can be found by Crandall et al. (1968) which also includes useful references. However, because of the technological state of art before 1990, the consideration of piezoelectric effect was limited to some field of applications in optics and electronics.

After that date, new energy transducers based on the piezoelectric effect became available being able to exert forces up to hundred Newtons; moreover, they are as light as few grams and their typical dimensions are of the order of centimeters (see for instance Near, 1996). Mathematical models describing their behavior are extensively discussed by Rogacheva (1994). How

these transducers can be used in structural mechanics is examined in Gandhi and Thompson (1992), Culshaw (1996) and Cudney et al. (1999).

The typical electro-mechanical structure damping of mechanical vibrations by means of an electrical and purely passive shunt is introduced by Hagood and von Flotow (1991) and Valis et al. (1991). The electric circuit connected to the piezoelectric transducer is resonant with a mechanical mode and its passive impedance supplies the damping device.

The aforementioned references only partially reflect the wide interest which has been devoted to the study of electro-mechanical coupling phenomena related to the use of piezoelectric actuators and sensors; for further details we quote Utku (1998) and Fuller et al. (1996). We explicitly remark that both the passive and active control methods can be used when exploiting piezoelectric transducers. In Fuller et al. (1996) the problem of active control is addressed, while in Hagood and von Flotow (1991) and Valis et al. (1991) only conservative devices are considered: the latter choice may be preferred when one needs intrinsically stable systems and/or structures which show an electromechanical response independent of the external excitation. However, we stress that conservative circuital elements can be synthesized using active elements.

In this paper the attention is focused on a class of electro-mechanical systems introduced in Vidoli and dell'Isola (2000, 2001), dell'Isola et al. (2001) and Alessandrini et al. (2001); a distributed technique for structural control is realized connecting a set of piezoelectric actuators through electric transmission lines or nets. Since the control system is designed to have the same governing differential equations of the mechanical system, a modal resonance is used to efficiently transduce the energy from the mechanical to the electrical form.

A preliminary linear analysis is worked out to better investigate the conditions of maximum coupling due to the gyroscopic terms: in the non-dissipative case, a veering phenomenon of the wave-speeds allows for the selection of a critical value of the parameters; in the dissipative case, a local maximum in the damping ratios indicates the region where an efficient dissipation of the mechanical energy takes place.

Here we analyze the effects, caused by the introduction of some nonlinear terms, on the interaction between an electrical and a mechanical mode. The nonlinearities concern the piezoelectric constitutive relation; indeed, as a result of their ferroelectric nature, piezoelectric materials exhibit hysteresis and nonlinear saturation effects, see for instance Smith and Ounaies (1999). As a first approximation we consider a one-to-one relation assuming a cubic dependence between the polarization and the applied electric field.

When the nonlinearity is considered, the numerical evidence shows a decreasing efficiency of the system in transducing energy near the critical linear condition; a different, but yet convenient, tuning of the electric parameters depending on the strength of the nonlinearity may, however, be used.

Finally, the possibility of a different mechanism of energetic exchange is investigated through the method of multiple scales. We look for a superharmonic resonance allowing for a relevant transformation of energy from the mechanical to electrical form.

2. Formulation of the problem

Two common features of the control systems presently used for vibration damping are the differentiation between the sensing and the actuation systems, and the localization of PZT actuators at a small number of specific sites on the vibrating structure. Both features are limits to the control efficiency. Indeed, the first one implies the need for high power in concentrated structural regions and the need for a coordinating active system that controls the actuator action in response to the input from the sensors. The latter implies an optimal localization problem (for both the actuators and sensors), the solutions of which actually depend on the particular mechanical vibration mode under consideration.

In order to bypass these problems in Vidoli and dell'Isola (2000, 2001), the concept of parallelism between mechanical structures and electric control systems is introduced: a structure is controlled by means of a uniform distribution of actuators connected through an electric transmission net. An internal resonance phenomenon between structural modes and electric modes is then exploited to optimize the control efficiency. A suitable tuning of the net impedance turns out to be the *tap* for the electro-mechanical coupling and for efficient energy transfer. These control systems allow for a strong control action and shorter energy transfer times between the electrical and mechanical forms. Moreover, net-control systems avoid the problems of the optimum positioning (of actuators and sensors) being able to manage all the mechanical modes through the same distributed configuration of its collocated actuators.

In dell'Isola et al. (2001) and Alessandroni et al. (2001), the electric analogs for the *Elastica* and the Kirchhoff-Love plate are synthesized and linear coupled electromechanical vibrations are studied. As forecast in Vidoli and dell'Isola (2001), the piezoelectric coupling of a structure with its electric analog is proven (in Alessandroni et al., [2]) to be able to efficiently control every

mechanical mode with the same choice of the electrical transmission impedance.

2.1. Description of the systems

We consider as a mechanical structure, to be controlled, the plate drawn in Figure 1, where the darker rectangular patches represent the piezoelectric actuators to be suitably interconnected via an electric circuit. We call $2h$ the thickness of the plate, ℓ and b its sides, and $d \ll \ell$ – the diameter of the influence region for each patch. When the ratio $b/\ell \ll 1$, and $b \simeq d$, the plate can be modelled as a beam.

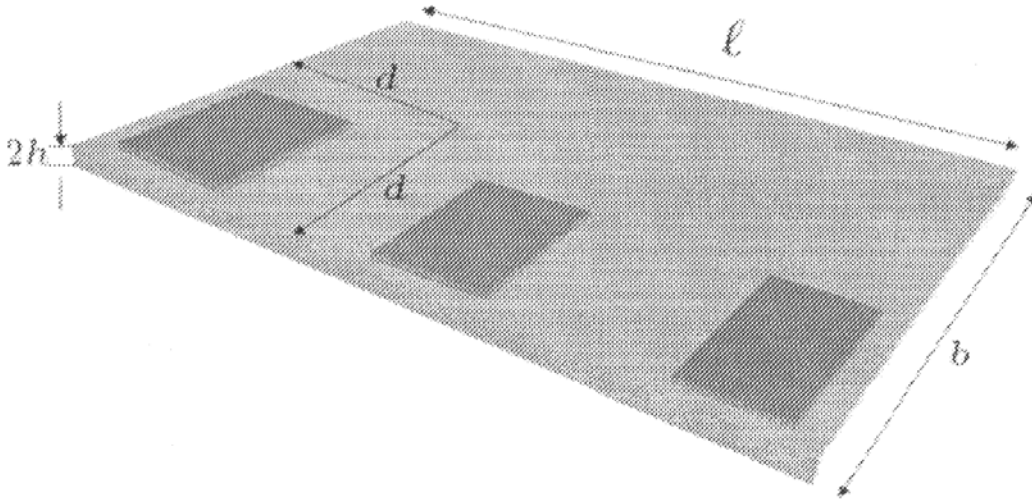


Fig. 1. Dimensions of the considered structures

The considered topologies of the electric interconnections will be those specified in the following Figures 2, 3, 4 and 5. In all the considered networks, the two-port capacitive elements represent the impedance of piezoelectric actuators, as the equivalent electrical circuit of a piezoelectric transducer is in a wide range of circumstances given by the parallel connection of a capacitor and a deformation – driven current generator; for a detailed discussion of this topic refer to Zelenka (1986).

The homogenized governing equations of the sketched networks respectively are:

- for Figure 2 the damped d'Alembert equation (Vidoli and dell'Isola, 2001);
- for Figure 3 the damped *Elastica* equation (Alessandroni et al., [2]);

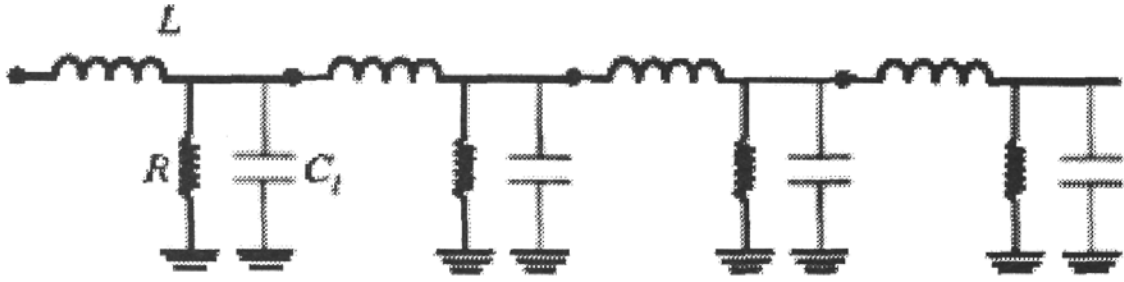


Fig. 2. Standard second order transmission line

- for Figure 4 the damped membrane equation (Vidoli and dell’Isola, 2001);
- for Figure 5 the damped Kirchhoff-Love plate equation (Alessandroni et al., [2]).

Remark that the circuits in Fig.3 and Fig.5, although governed by conservative equations, are constituted by some active elements, i.e. the negative inductances. These latter can be synthesized for instance using gyrators or the Antoniou circuit. However, the stability of the considered electric networks is assured once the employed active elements (which in general will be operational amplifiers) behave linearly.

Here we investigate those situations, occurring in the presence of high polarization voltages, in which the piezoelectric actuators could show a nonlinear or eventually hysteretic behavior (Smith and Ounaies, 1999). Therefore the evolution equations for the proposed electro-mechanical systems become nonlinear. In the performed analysis we limit our attention to a cubic nonlinear electric constitutive relation between the applied voltage $\dot{\phi}$ and the polarization P in the piezoelectric elements

$$P = C_1 \dot{\phi} - C_3 \dot{\phi}^3 \quad C_1 > 0 \quad C_3 > 0 \quad (2.1)$$

as a consequence, the constitutive relation for the piezoelectric bending actuators becomes

$$\begin{bmatrix} M \\ P \end{bmatrix} = \begin{bmatrix} k_{mm} & k_{me} \\ -k_{me} & C_1 \end{bmatrix} \begin{bmatrix} \chi \\ \dot{\phi} \end{bmatrix} - \begin{bmatrix} 0 \\ C_3 \dot{\phi}^3 \end{bmatrix}$$

where M and χ are the bending moment and curvature, respectively. Other nonlinearities will be addressed in subsequent investigations, for instance following the ideas discussed in Richard et al. (1999).

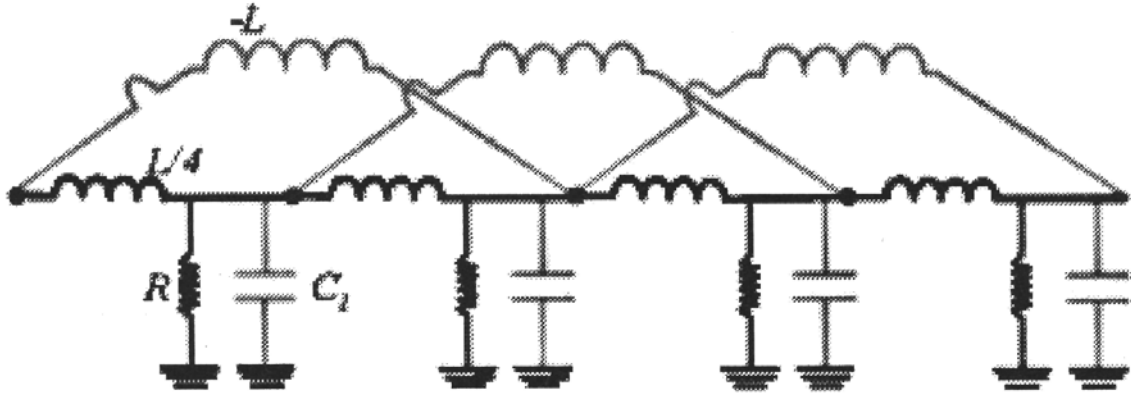


Fig. 3. Fourth order transmission line

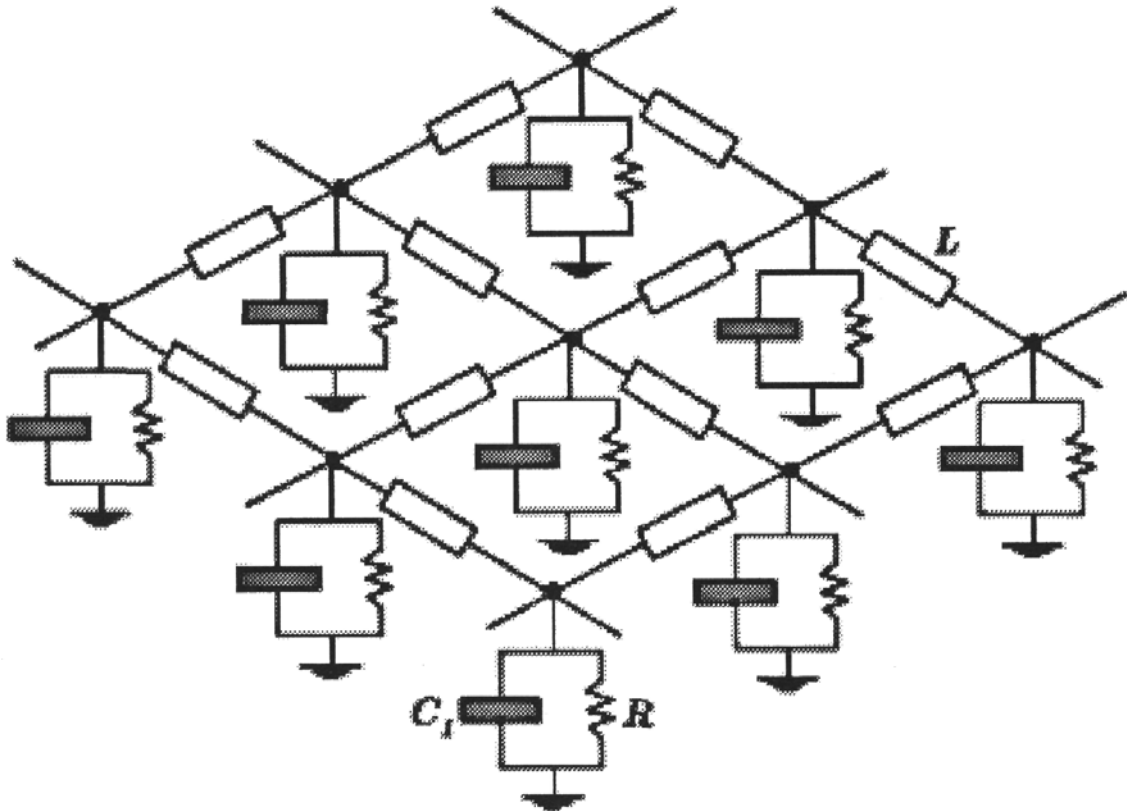


Fig. 4. Second order transmission net

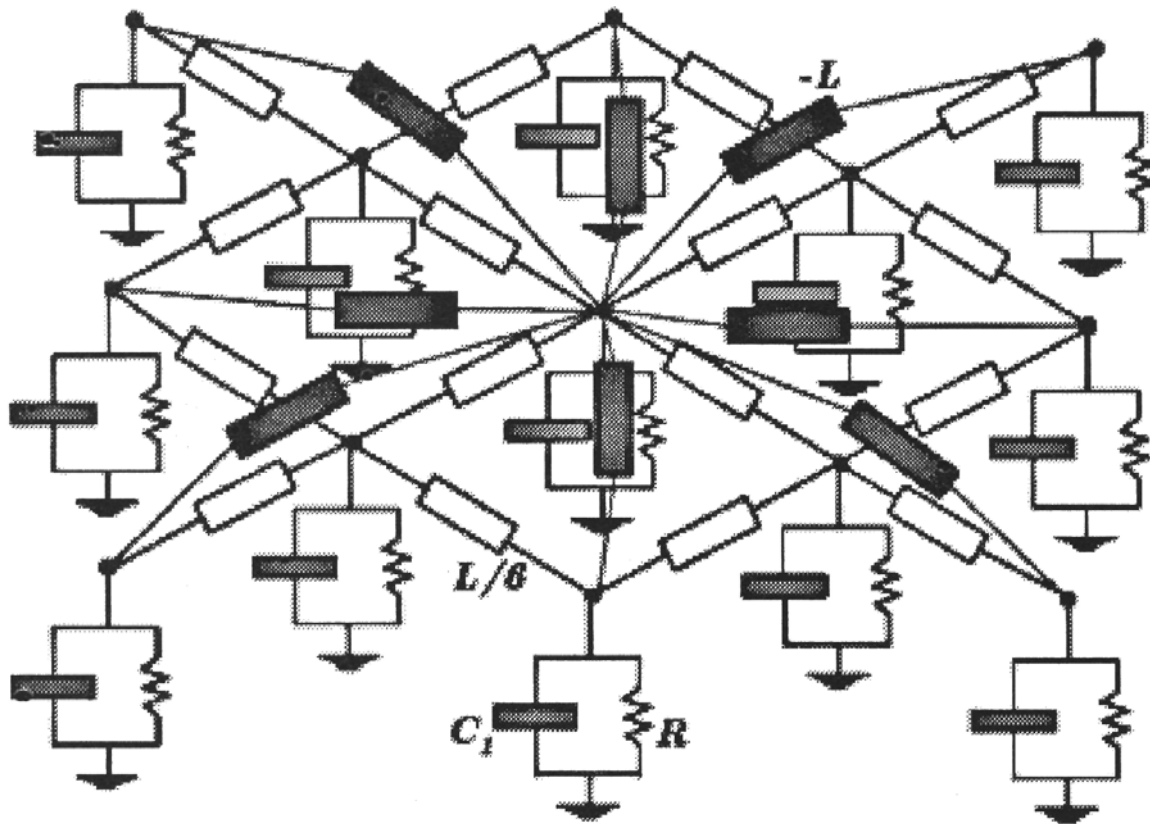


Fig. 5. Fourth order transmission net

2.2. Modal analysis

The introduced electromechanical system needs to be designed in order to optimize its mechanical damping performances. Indeed, the concept on which it is based consists in a multiple internal electromechanical resonance. Such an optimization procedure becomes arduous if the analysis is attempted for a lumped electric network connected to a continuous structural member; in this case one should use a numerical solution for a system of coupled PDEs with a set of Lagrangian ODEs in a wide range of electrical parameters and initial data. Instead we have chosen to homogenize the governing equations of the electric network and perform a quasi-analytical optimization for a set of coupled PDEs. This is a standard approximate analysis often used in structural mechanics (Woźniak, 1993).

All the considered net-control systems are governed by partial differential equations of the following type

$$\begin{aligned} \mathbf{A}(u) + \ddot{u} - \mathbf{C}(\dot{\phi}) &= 0 \\ \mathbf{B}(\phi) + \ddot{\phi} + \mathbf{C}^*(\dot{u}) + D\dot{\phi} &= \epsilon\ddot{\phi}\dot{\phi}^2 \end{aligned} \quad (2.2)$$

Here u and ϕ stand for the mechanical displacement and an electric potential time-integral, respectively. Thus the operators \mathbf{A} , \mathbf{B} and \mathbf{C} physically mean the mechanical operator (accounting for the structural mass and stiffness), the electrical operator (accounting for the net inductance and capacitance) and the coupling operator (accounting for the piezoelectric effect). From a mathematical point of view, \mathbf{A} and \mathbf{B} are linear self-adjoint and positive definite operators, while \mathbf{C} is required to be simply linear. Finally D and ϵ are scalars representing the net resistance and nonlinearity coefficient respectively, and a superscript $*$ is used to indicate the adjoint operator.

In the following table the corresponding operators are associated to the electrical networks and underlying structures.

	$\mathbf{A}(u)$	$\mathbf{B}(\phi)$	$\mathbf{C}(\dot{\phi})$
Fig. 2	u^{IV}	ϕ''	$\dot{\phi}''$
Fig. 3	u^{IV}	ϕ^{IV}	$\dot{\phi}''$
Fig. 4	$\Delta\Delta u$	$\Delta\phi$	$\Delta\dot{\phi}$
Fig. 5	$\Delta\Delta u$	$\Delta\Delta\phi$	$\Delta\dot{\phi}$

Eqs (2.2) are projected on a basis of eigenfunctions ψ_i and χ_j for the operators \mathbf{A} and \mathbf{B} . If

$$\langle \mathbf{C}(\chi_j), \psi_i \rangle = \langle \chi_j, \mathbf{C}^*(\psi_i) \rangle \quad i \neq j$$

are negligible¹, then it is possible to study, instead of (2.2), a sequence of ODEs of the type

$$A_i u_i + \ddot{u}_i + C_i \dot{\phi}_i = 0 \quad (2.3)$$

$$B_i \phi_i + \ddot{\phi}_i - C_i \dot{u}_i + D_i \dot{\phi}_i + C_i D_i u_i + \sum \epsilon_{ijkl} \ddot{\phi}_j \dot{\phi}_l \dot{\phi}_k = 0$$

where

$$\epsilon_{ijkl} := \langle \chi_j \chi_l \chi_k, \chi_i \rangle$$

and no sum over the repeated index i is understood. In what follows we will omit the index i and limit our attention to the study of the influence on

¹As proven in Vidoli and dell'Isola (2001) such a condition can be verified suitably choosing the boundary conditions for the electric net.

the i th mode of the nonlinearity arising from ϵ_{iiii} only, postponing a more detailed analysis to further investigations. The performed analysis will be well-grounded when the frequencies $\varpi_j \pm \varpi_l \pm \varpi_k$ are not resonant with ϖ_i , being $\varpi_h := \sqrt{B_h}$ for $h = j, l, k, i$.

The eigenbases used to get the coefficients in (2.3) will be

$$\psi_i(x) = \chi_i(x) = \sqrt{2} \sin(i\pi x) \quad x \in [0, 1] \quad (2.4)$$

for the beam, and

$$\begin{aligned} \psi_i(x, y) \equiv \chi_i(x, y) &= \frac{2}{\sqrt{\eta}} \sin(h_i x) \sin \frac{k_i y}{\eta} \\ x \in [0, 1] \quad y \in [0, \eta] \quad \eta &:= \frac{b}{\ell} \end{aligned} \quad (2.5)$$

for the plate. The indices h_i and k_i which determine the modal forms are defined according to the following table

		Modes labeling								
		$i = 1$	2	3	4	5	6	7	8	9
h_i		1	1	2	2	1	3	2	3	3
k_i		1	2	1	2	3	1	3	2	3

The following tables will allow for the identification of the parameters appearing in (2.3) for all the considered PEM structures:

	A	B	C
Second order line (Fig. 2)	i^4	$i^2 \frac{d\ell M}{\pi^2 LC_1 D_B}$	$i^2 g_{med} d \sqrt{\frac{b}{C_1 D_B}}$
Fourth order line (Fig. 3)	i^4	$i^4 \frac{d^4 M}{\ell LC_1 D_B}$	$i^2 g_{med} d \sqrt{\frac{b}{C_1 D_B}}$
Second order net (Fig. 4)	$(h_i^2 + k_i^2)^2$	$(h_i^2 + k_i^2) \frac{d^2 \ell M}{\pi^2 b LC_1 D_P}$	$(h_i^2 + k_i^2) g_{med} d \sqrt{\frac{1}{C_1 D_P}}$
Fourth order net (Fig. 5)	$(h_i^2 + k_i^2)^2$	$(h_i^2 + k_i^2)^2 \frac{d^4 M}{\ell b LC_1 D_P}$	$(h_i^2 + k_i^2) g_{med} d \sqrt{\frac{1}{C_1 D_P}}$

	D	ϵ
Second order line (Fig. 2)	$\frac{\ell^2}{\pi^2 RC_1} \sqrt{\frac{M}{D_B \ell}}$	$\frac{9}{2} \frac{\pi^4 C_3 d^4 D_B}{C_1^2 \ell^4 b}$
Fourth order line (Fig. 3)	$\frac{\ell^2}{\pi^2 RC_1} \sqrt{\frac{M}{D_B \ell}}$	$\frac{9}{2} \frac{\pi^4 C_3 d^4 D_B}{C_1^2 \ell^4 b}$
Second order net (Fig. 4)	$\frac{\ell^2}{\pi^2 RC_1} \sqrt{\frac{M}{D_P \ell b}}$	$\frac{81}{4\eta} \frac{\pi^4 C_3 d^4 D_P}{C_1^2 \ell^4}$
Fourth order net (Fig. 5)	$\frac{\ell^2}{\pi^2 RC_1} \sqrt{\frac{M}{D_P \ell b}}$	$\frac{81}{4\eta} \frac{\pi^4 C_3 d^4 D_P}{C_1^2 \ell^4}$

The meanings of the symbols are specified by:

Symbol	Name
g_{me}	piezoelectric coupling coefficient [N/V]
M	beam or plate mass [Kg]
D_B, D_P	beam, plate bending stiffnesses [Nm ² , Nm]
η	aspect ratio of the plate [b/ℓ]
L	inductance [H]
R	resistance [Ω]
C_1	capacitance [F]
C_3	capacitance [F/V ²]

The displacement was made dimensionless with respect to d and the time-integral $\dot{\phi}$ of the electric potential with respect to $d^2 \sqrt{M/(C_1 \ell b)}$.

The parameter B can be electrically tuned and it is actually used to get the maximum dynamical coupling between the modes (suggestive animations showing this tuning procedure can be found at <http://www.disg.uniroma1.it/ncs>). Incidentally, high values of the parameter B are preferable, since the production of high inductances is of a high technological cost.

Finally note that the ratio B/A for the fourth-order line and net (Fig. 3 and Fig. 5) is independent of the mode number; this means that a unique tuning of the electric parameters in B allows to control all the modes of the continuum structure (beam or plate).

3. Linear spectral properties

3.1. Non-dissipative case: eigenfrequencies

The linear problem is obtained in the limit for $\epsilon \rightarrow 0$. First of all we analyze the non-dissipative case when the parameter D vanishes

$$\begin{aligned} Au + \ddot{u} + C\dot{\phi} &= 0 \\ B\phi + \ddot{\phi} - C\dot{u} &= 0 \end{aligned} \quad (3.1)$$

For A and B being real positive numbers, the system is conservative. Thus the roots of the characteristic polynomial

$$s^2C^2 + (s^2 + A)(s^2 + B) = 0 \quad (3.2)$$

are pairs of conjugate imaginary numbers $s = \pm\omega_i$

$$\omega_1 = \sqrt{\frac{1}{2}[(C^2 + A + B) + \delta]} \quad \omega_2 = \sqrt{\frac{1}{2}[(C^2 + A + B) - \delta]} \quad (3.3)$$

where

$$\delta = \sqrt{(C^2 + A + B)^2 - 4AB}$$

when $C \rightarrow 0$ then $\omega_1 \rightarrow \sqrt{A}$ and $\omega_2 \rightarrow \sqrt{B}$.

Figure 6 shows the two eigenfrequencies ω_i as functions of the ratio B/A and for the fixed value $C = \sqrt{A/50}$ of the coupling coefficient; the colors (yellow and blue) mean the nature of the associated eigenvector (mechanical and electrical respectively). The m , e and em subscripts are also used to indicate the same fact. In Fig. 6 the dashed lines represent the eigenfrequencies computed for a vanishing value of the coupling parameter C ; in this case, the two loci of frequencies cross each other and do not interact.

There is a range of the ratio B/A (namely around 1) where all the eigenvectors have components of comparable energy: in this range there is no wave purely mechanical or purely electrical. This is a typical behavior of systems characterized by veering phenomena in the eigenfrequencies curves (Perkins and Mote, 1986; Vidoli and Vestroni [20]).

In Figure 7 both the eigenfrequencies ω_i and the eigenvectors are plotted as functions of the parameter B ; the dashed curves refer to the uncoupled case ($C = 0$). It is evident how the, initially mechanical, eigenvector $\{u_1, u_2\}|_{B=0} \simeq \{1, 0\}$ continuously transforms into the electric eigenvector $\{u_1, u_2\}|_{B \rightarrow \infty} \simeq \{0, 1\}$ and vice versa; the region in which all the eigenvector

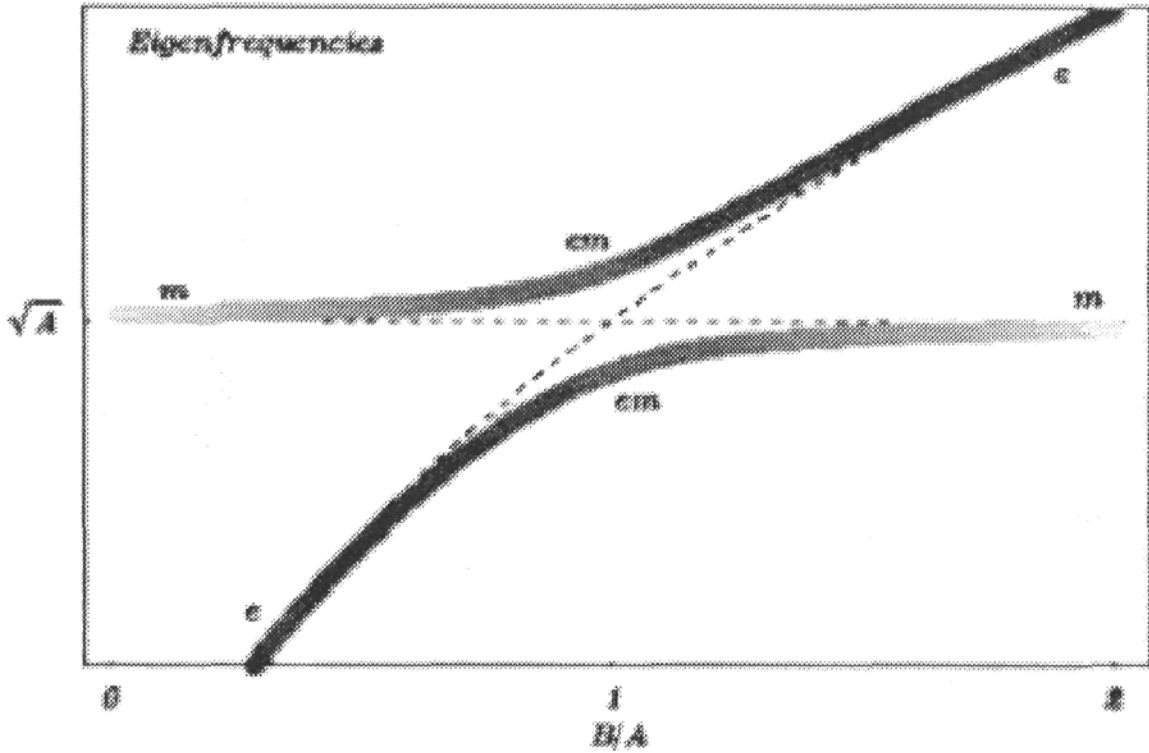


Fig. 6. Veering of eigenfrequencies

components have comparable values is called veering region and labeled by the letter σ . In Vidoli and Vestroni [20] the length σ is estimated by means of the analytical representation of the eigenvectors for different kinds of coupling, namely elastic, gyroscopic and inertial.

Thus when $B \simeq A$, the electro-mechanical coupling is maximum; a time-evolution problem starting from purely mechanical initial data leads to a back and forth exchange of energy between the mechanical and electrical forms as shown in Figure 8. Four different kinds of energies are involved: the mechanical elastic energy ($Au^2/2$), the kinetic energy ($\dot{u}^2/2$), the electric inductive energy ($B\dot{\phi}^2/2$) and the electric capacitive energy ($\phi^2/2$). The total energy is constant since we are considering the non-dissipative case. The time interval $T = \pi/|\omega_1 - \omega_2|$ represents the time elapsed for a complete transfer of energy between the mechanical and electrical forms.

3.1.1. Diagonalization

In order to perform a nonlinear analysis of Eqs (2.3) we find it useful to diagonalize its linear part. Due to the presence of the gyroscopic terms, the linear isomorphism $\Upsilon : (u, \phi) \rightarrow (\eta_1, \eta_2)$ that transforms the linear part of the

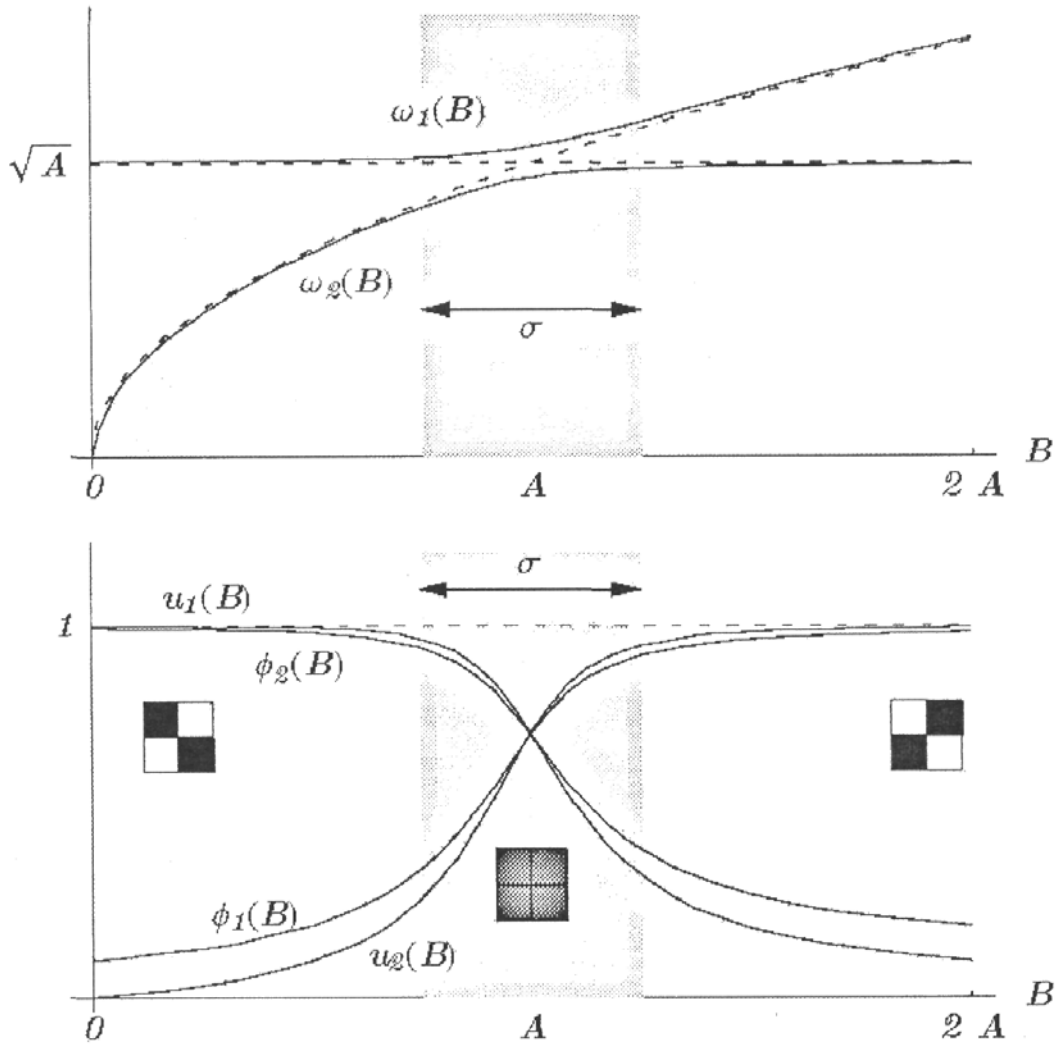


Fig. 7. Behavior of eigenfrequencies and eigenvectors near veering

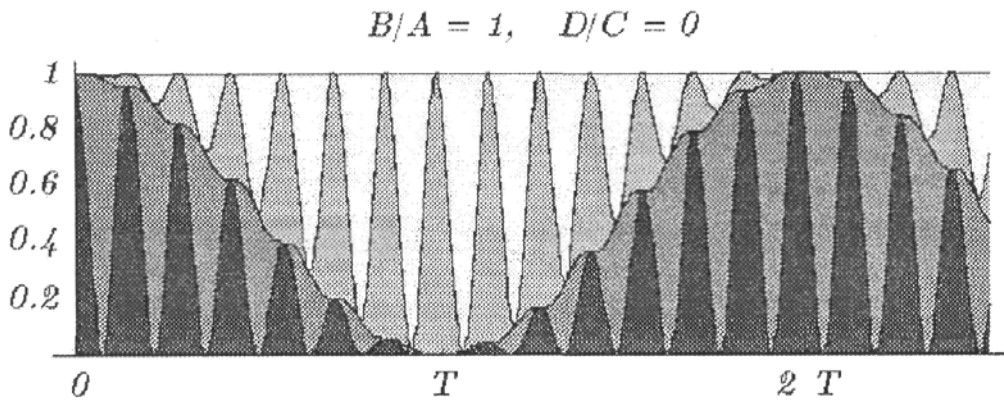


Fig. 8. Time evolution of mechanical and electric energies (non-dissipative case)

system (2.3) with D vanishing, in the standard diagonal form

$$\ddot{\eta}_i + \omega_i^2 \eta_i = 0 \quad i = 1, 2$$

necessarily involves the time-derivative operator. Thus the system can be diagonalized only in the state-space through the linear transformation

$$\begin{bmatrix} \eta_1 \\ \eta_2 \\ \dot{\eta}_1 \\ \dot{\eta}_2 \end{bmatrix} = \begin{bmatrix} 0 & c_1 & c_2 & 0 \\ 0 & c_3 & -c_2 & 0 \\ -Ac_2 & 0 & 0 & c_4 \\ Ac_2 & 0 & 0 & c_5 \end{bmatrix} \begin{bmatrix} u \\ \phi \\ \dot{u} \\ \dot{\phi} \end{bmatrix} \quad (3.4)$$

where

$$\begin{aligned} c_1 &= \frac{B(-A + B + C^2 + \delta)}{\delta(A + B + C^2 + \delta)} & c_2 &= \frac{C}{\delta} \\ c_3 &= -\frac{B(-A + B + C^2 - \delta)}{\delta(A + B + C^2 - \delta)} & c_4 &= \frac{2AC^2}{\delta(A - B - C^2 + \delta)} \\ c_5 &= \frac{2AC^2}{\delta(-A + B + C^2 + \delta)} \end{aligned} \quad (3.5)$$

3.2. Dissipative case: damping ratios

When the net resistance D does not vanish, the system is dissipative; the characteristic polynomial is

$$s^2 C^2 + (s^2 + A)(s^2 + sD + B) = 0 \quad (3.6)$$

the complex roots of this polynomial physically represent the damping ratios (real parts) and the pulsations (imaginary parts) of the waves.

In Figure 9 the damping ratios are drawn as functions of the ratio D/C for $B = A$; again we use the colors and the letters m and e to indicate the nature of the associated eigenvectors. The presence of a maximum value for the lower branch of the damping ratios is evident, the electric dissipation (namely the resistance parameter D) should be large enough to dissipate energy but small enough to allow for the electro-mechanical transduction. The dashed line is the locus of points $\{D/C, D/4C\}$; thus the maximum mechanical damping ratio of about $0.5C$ is attained when $D \simeq 2C$.

Once the optimal values for the parameters are chosen, the time-evolution from a mechanical initial data shows an efficient energy dissipation, Fig. 10. Indeed, the part of mechanical energy transformed into the electric form is damped and can not return anymore in the mechanical system.

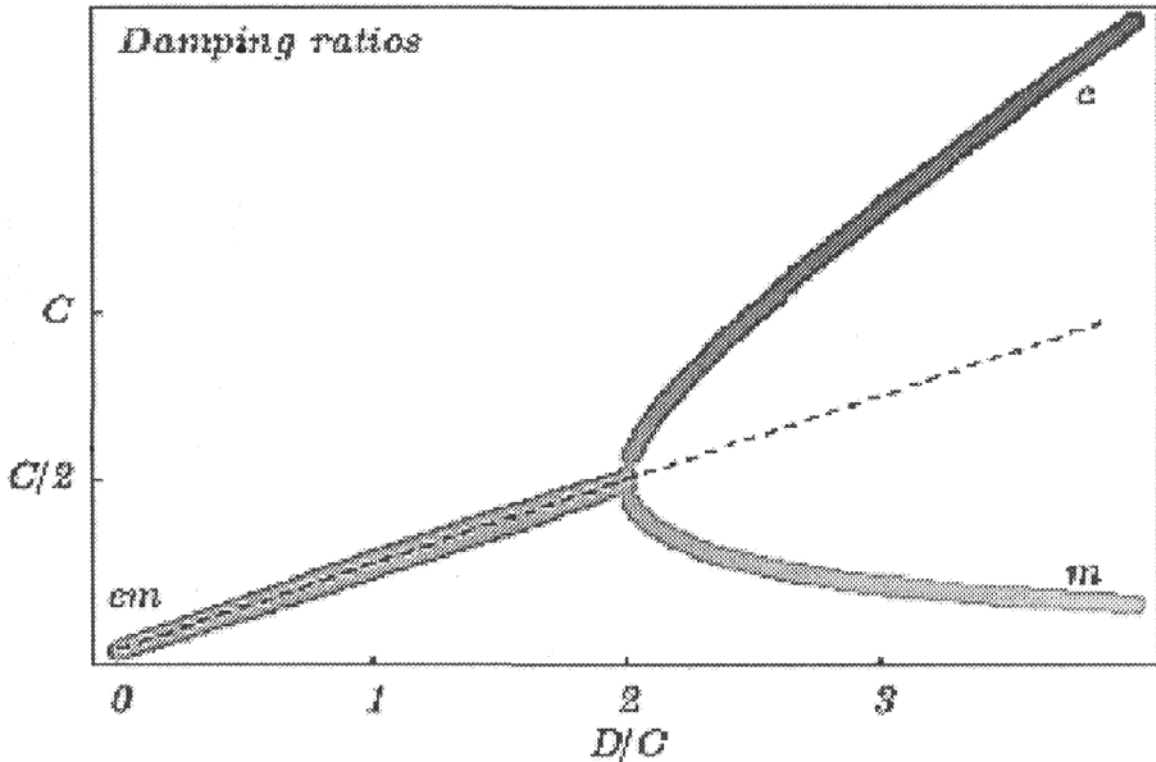


Fig. 9. Damping ratios versus D/C for $B = A$

4. Nonlinear analysis

4.1. Numerical evidence

The effects of the nonlinearity on the energy exchange between electrical and mechanical forms have been analyzed integrating numerically Eqs (2.3).

For fixed values of the coupling coefficient ($C = \sqrt{A/50}$) and of the net resistance ($D = C/2$), the dissipation of total energy after a time period $T = \pi/|\omega_1 - \omega_2|$, which is the time elapsed for a complete transfer of energy in the linear non-dissipative case, has been computed for a wide range of the parameters ϵ and B/A : the results are shown in Figure 11.

As expected, the optimal value of the electric parameter B/A is different and depends on the intensity of the nonlinearity ϵ . In Figure 11 the dashed curve represents this optimal value B/A as a function of ϵ , evaluated numerically for a vanishing value of the electric dissipation D . The monotonic increase of this optimal curve with respect to the strength of the nonlinearity ϵ is a convenient situation, since it involves lower values of the optimal inductance. Also note that for high values of the nonlinearity, the level of dissipated energy tends

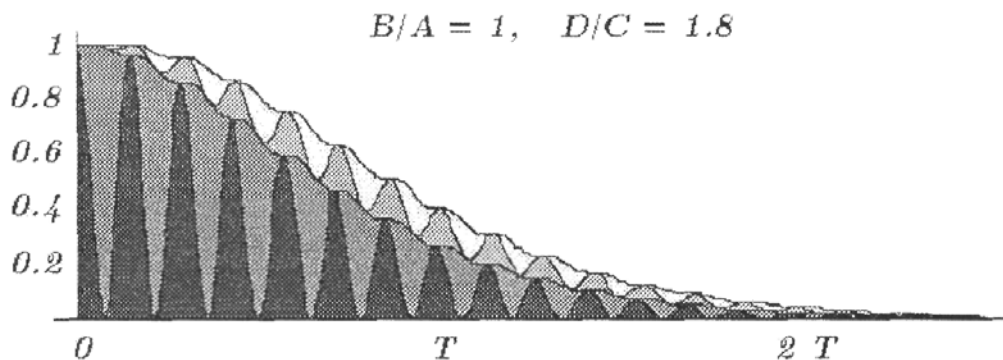


Fig. 10. Time evolution of mechanical and electric energies (dissipative case)

to be low; indeed, as Figure 12 also shows, there exists a nonlinearity threshold beyond which the complete energy transfer is not possible anymore: again more details and animations can be found at <http://www.disg.uniroma1.it/ncs>.

In the first column of Figure 12 the time histories of the energies are computed in the non-dissipative case; the darker regions represent the amount of mechanical, both kinetic and potential, energy. The time intervals elapsed for a complete transformation of the energy are longer than in the linear case, but these transformations are achieved through lower values of the net inductance.

Also the optimal value of net resistance, that maximizes the energy dissipation, increases with respect to the intensity of the nonlinearity; indeed, in Figure 11b the darkness is proportional to the energy dissipation. From a technological point of view, this is a favorable situation since the production of inductances with low associated resistances is of a high technological cost.

In the second column of Figure 12 the time histories of the energies in the dissipative case confirm the aforementioned conclusions: the time needed to damp the vibration is sensibly larger even if it is obtained through a more favorable tuning of the electric parameters.

4.2. Multiple scales approximation

Since, in the linear case, the energy transduction is essentially based on an internal resonance phenomenon $\omega_1 \simeq \omega_2$, the cubic nonlinearity, affecting the electric frequency, progressively destroys the resonance condition. Thus for high values of the parameter ϵ , the energy transduction is negligible and it is preferable to seek for a different mechanism of energetic exchange. To this end, led by the cubic nature of the nonlinearity, we investigate by an asymptotic method the case of a three-to-one internal resonance.

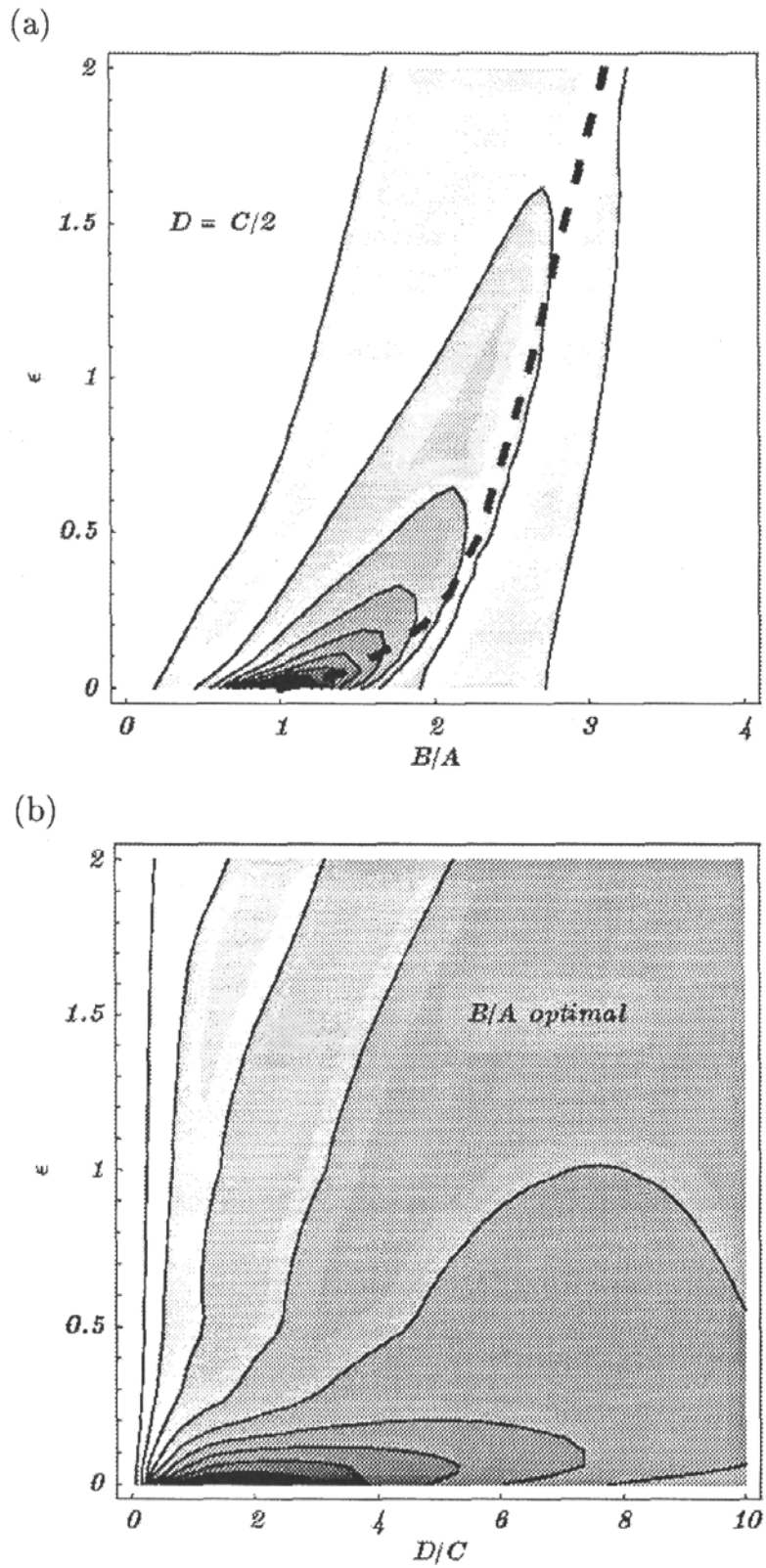


Fig. 11. Energy dissipation as function of (a) B/A and ϵ ; (b) D/C and ϵ . In the darker regions the dissipation is higher

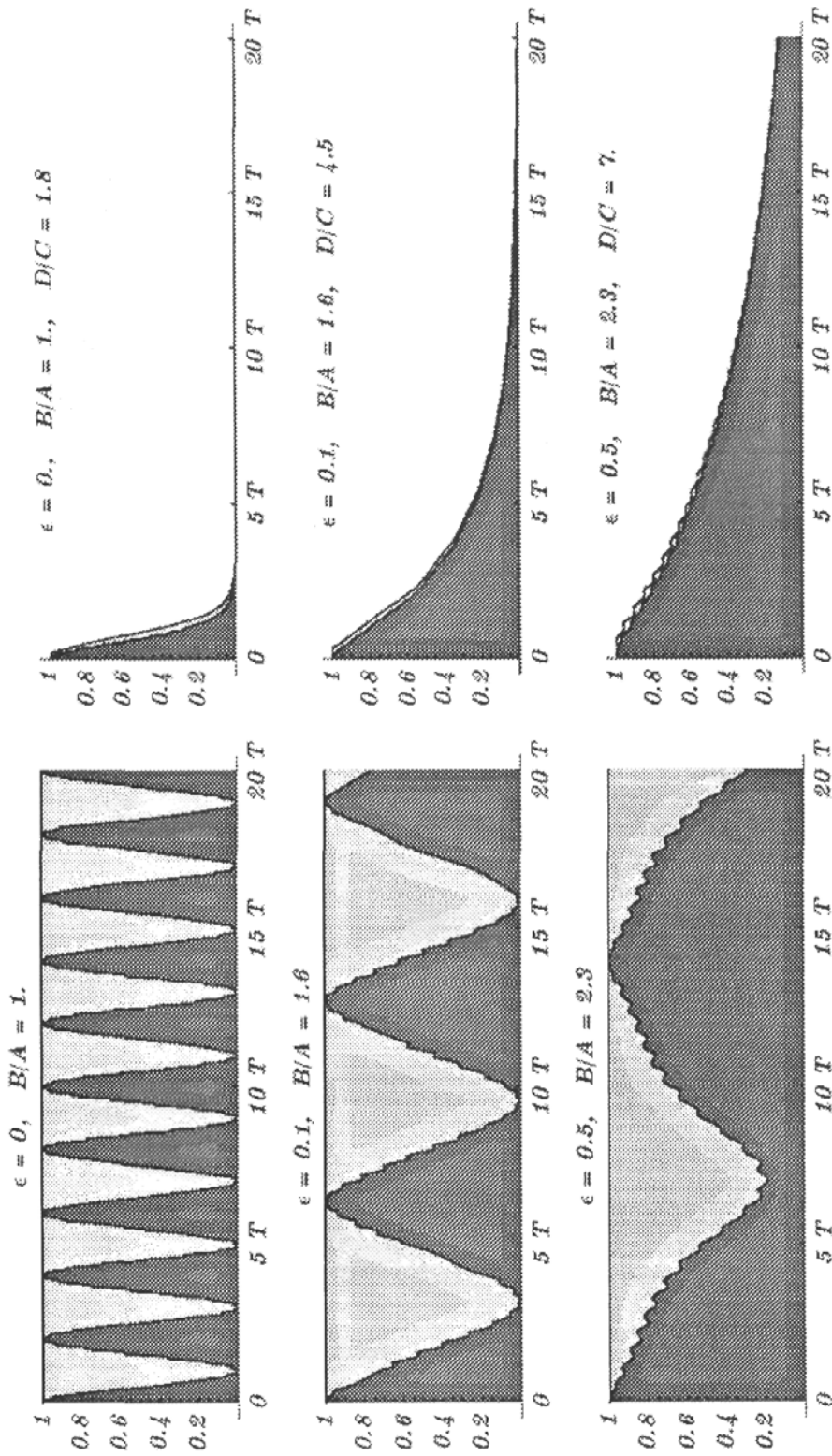


Fig. 12. Time evolutions of the electric and mechanical energies for different values of ϵ and optimal value B/A . The first column refers to the conservative case, the second to the dissipative case

First of all, by means of the linear transformation (3.4) the nonlinear system is transformed into

$$\begin{aligned} \ddot{\eta}_1 + \omega_1^2 \eta_1 &= 3\epsilon c_4 (\dot{\eta}_1 + \dot{\eta}_2)^2 (\ddot{\eta}_1 + \ddot{\eta}_2) \\ \ddot{\eta}_2 + \omega_2^2 \eta_2 &= 3\epsilon c_5 (\dot{\eta}_1 + \dot{\eta}_2)^2 (\ddot{\eta}_1 + \ddot{\eta}_2) \end{aligned} \tag{4.1}$$

The solution is found using the method of multiple scales (Nayfeh, 1981), i.e.

$$\begin{aligned} T_0 &:= t & T_1 &:= \epsilon t \\ \eta_i(t, \epsilon) &\simeq \eta_i^{(1)}(T_0, T_1) + \epsilon \eta_i^{(2)}(T_0, T_1) + \dots \end{aligned} \tag{4.2}$$

for $i = 1, 2$. The three-to-one resonance condition is achieved when $\omega_1 \simeq 3\omega_2$.

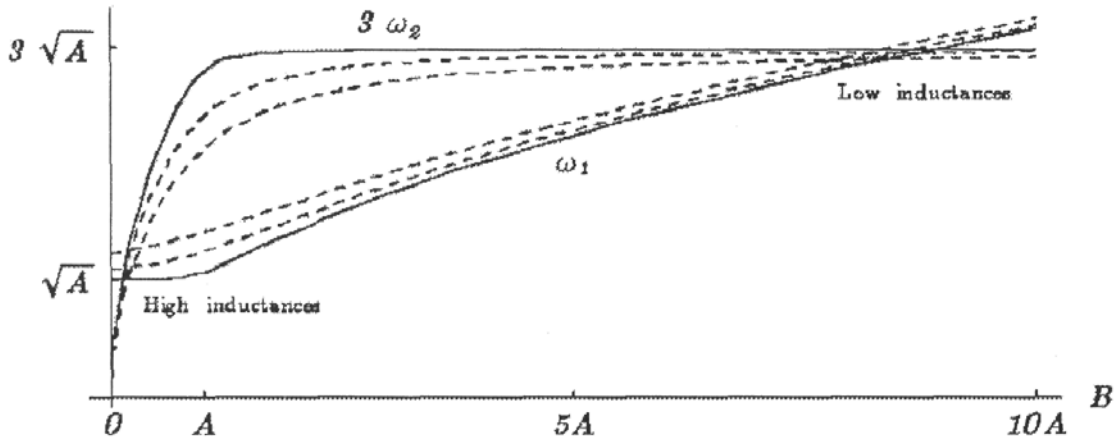


Fig. 13. Solutions for the three-to-one resonance in terms of inductance

For every choice of A and C this condition is verified by two possible values for B ; refer to the following table and Figure 13 (computed for $A = 4\pi^2$ and different values of C)

$C = \sqrt{A/50}$	$B = 8.995 A$	or	$B = 0.116 A$
$C = \sqrt{A/5}$	$B = 8.543 A,$	or	$B = 0.169 A$
$C = \sqrt{A/2}$	$B = 7.824 A,$	or	$B = 0.288 A$

Incidentally note that, from Eqs (3.3), the condition $\omega_2 \simeq 3\omega_1$ can not be achieved by any choice of the parameters.

The modulation equations for the amplitudes a_i and phases β_i of the first-order solution

$$\eta_i^{(1)}(T_0, T_1) = a_i(T_1) \cos[\omega_i T_0 + \beta_i(T_1)] \quad (4.3)$$

are found as follows

$$\begin{aligned} a_1'(T_1) &= -\frac{3c_4\omega_2^4}{8\omega_1}a_2^3 \sin \gamma \\ a_2'(T_1) &= \frac{3c_5\omega_2\omega_1(\omega_1 - 2\omega_2)}{8}a_2^2 a_1 \sin \gamma \\ \gamma'(T_1) &= \sigma + \frac{9(2c_4 - c_5)\omega_2^3}{8}a_2^2 + \left(\frac{27c_5 a_2 a_1}{8} - \frac{c_4 a_2^3}{8a_1}\right)\omega_2^3 \cos \gamma + \\ &\quad + \frac{81(c_4 - 2c_5)\omega_2^3}{8}a_1^2 \end{aligned} \quad (4.4)$$

where $\gamma = \beta_1 - 3\beta_2 + \sigma T_1$ and we have introduced a detuning parameter σ such that $\omega_1 = 3\omega_2 + \epsilon\sigma$. Two stationary solutions of the modulation equations (4.4) are analytically found

$$\begin{cases} \sin \gamma = 0 \Rightarrow \gamma = n\pi \\ \sigma + \frac{9(2c_4 - c_5)\omega_2^3}{8}a_2^2 \pm \frac{27c_5\omega_2^3}{8}a_1 a_2 \pm \frac{c_4\omega_2^3}{8a_1}a_2^3 + \frac{81(c_4 - 2c_5)\omega_2^3}{8}a_1^2 = 0 \end{cases} \quad (4.5)$$

$$\begin{cases} a_2 = 0 \\ \sigma + \frac{81(c_4 - 2c_5)\omega_2^3}{8}a_1^2 = 0 \end{cases}$$

While Eq. (4.5)₂ represents a unimodal solution and, as a consequence, it does not involve energetic exchanges, the solution (4.5)₁ is satisfied by non-vanishing values of both the amplitudes a_1 and a_2 . In Figure 14 the solutions relative to Eqs (4.5)₁ are plotted for different values of the coupling parameter C and for the corresponding values of $B < A$ leading to a three-to-one resonance; the white (black) regions represent the regions of stable (unstable) solutions.

Increasing the coupling parameter C , two new branches of solutions arise. This is shown in detail in Figure 15 where the gray and black branches respectively, represent unstable and stable solutions.

When the three-to-one resonance is achieved with values of B greater than A , the stationary solutions given by Eqs (4.5)₁ are depicted in Figure 16. In

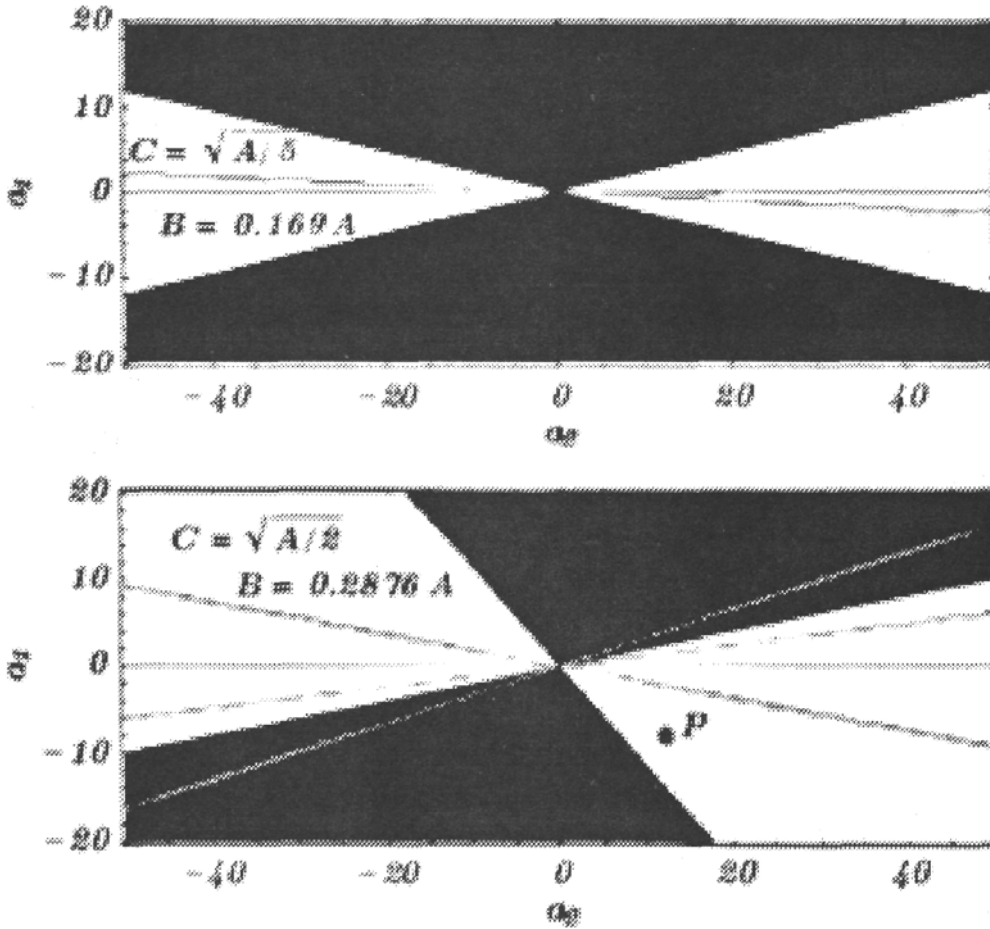


Fig. 14. Regions of instability (black) and stationary solutions (for $B < A$)

this case, for every value of the coupling parameter the only stationary solution is almost unimodal: the ratio between the amplitudes a_1/a_2 is, in fact, about $1/20$.

Since stationary solutions of the modulation equations correspond to periodic solutions of Eqs (4.1) that do not involve exchanges of energy, we are interested in stable solutions that are far from the stationary solutions. It is easy to verify that the choice of a point $P := (a_{1P}, a_{2P})$ in the plane of the amplitudes, corresponds to a choice of the initial conditions for $u(t)$ and $\phi(t)$ that satisfy

$$\frac{\dot{u}_0}{\phi_0} = \frac{1}{2C} \left[A - B + C^2 + \frac{\delta(m-1)}{m+1} \right] \quad m := \tan \frac{a_{1P}}{a_{2P}} \quad (4.6)$$

In Figure 17 the time-history of the mechanical displacement u and of the electric potential time-integral ϕ is shown; the initial conditions are relative to the point P in Figure 14.

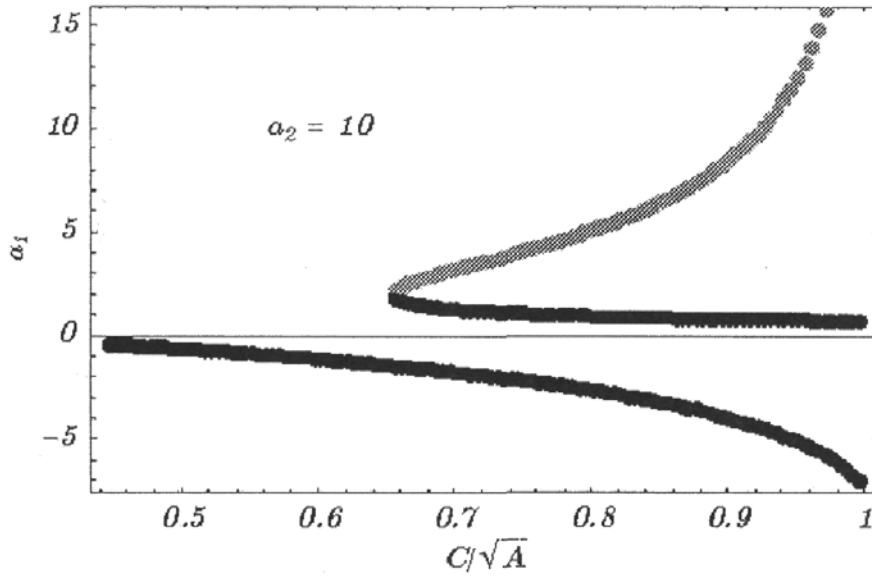


Fig. 15. Bifurcation of periodic solution (gray means an unstable solution)

We note that a relevant energy exchange takes place; also the time period of the energy transformation is sensibly shorter than in the linear case. However, we must remark a technological difficulty to realize this dynamical condition; in fact, the available piezoelectric actuators are characterized by a coupling coefficient C/\sqrt{A} in the range $0.01 \div 0.05$, while the new branch of sensibly coupled periodic solutions arises when $C/\sqrt{A} \simeq 0.7$.

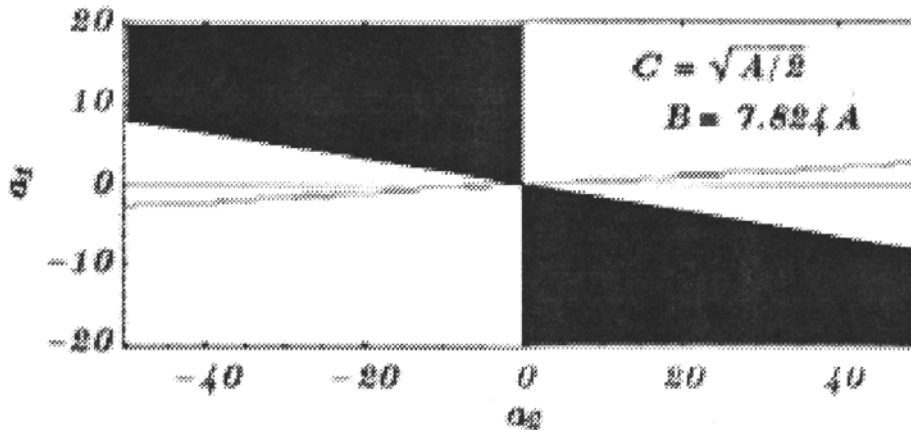


Fig. 16. Regions of instability (black) and stationary solutions (for $B > A$)

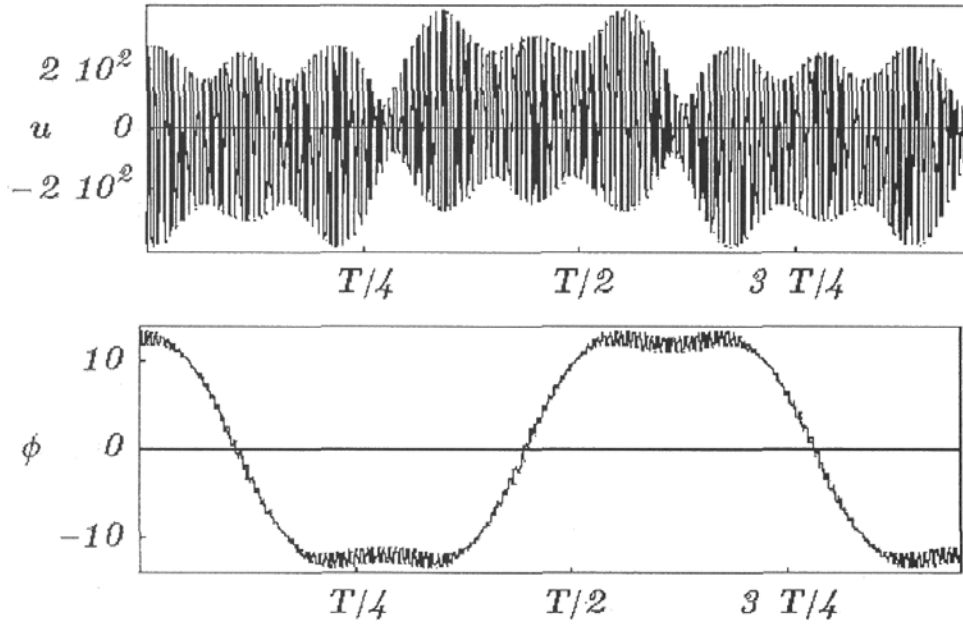


Fig. 17. Time evolution of u and ϕ with initial conditions in P ($C = \sqrt{A/2}$, $B = 0.288A$)

5. Conclusions

The dynamics of a coupled electro-mechanical system has been analyzed in order to find optimal values of its electrical parameters and increase its efficiency to control mechanical vibrations. Some effects of a cubic nonlinearity in the constitutive relation of the piezoelectric actuators have been considered.

An efficient transfer of energy is obtained, in the linear range, through a veering phenomenon ($\omega_2 \simeq \omega_1$). Under the same conditions, a purely electric dissipation damps the mechanical vibration.

The introduction of the cubic nonlinearity apparently decreases the system performances in terms of the dissipated energy and also increases the time interval needed for a complete energy transformation. On the other hand, it allows for a more convenient tuning of the net inductance and net resistance.

Moreover, the nonlinearity allows for a different mechanism of energetic transformation in the range of a super-harmonic resonance (namely $\omega_1 \simeq 3\omega_2$), which has been investigated by the method of multiple scales. It is found that a relevant energetic transformation can be obtained only with high values of the piezoelectric coupling coefficient, technologically unavailable today, and with a tuning of the net inductance about four times larger than in the linear case.

Although the previous considerations could be valid for a wider class of electromechanical systems, in particular for those in which the electric network is analogous to the structural member (Alessandroni et al., [2]), we postpone any conclusions concerning this problem to further investigations.

References

1. ALESSANDRONI S., DELL'ISOLA F., FREZZA F., 2001, Optimal piezomechanical coupling to control plate vibrations, *Proceedings ISEM, Tokyo 2001, to appear in Journal of Applied Electro-Magnetism and Mechanics*
2. ALESSANDRONI S., DELL'ISOLA F., PORFIRI M., A revival of electric analogs for vibrating mechanical systems aimed to their efficient control by PZT actuators, submitted for publication
3. CRANDALL S.H., KARNOPP D.C., KURTZ E.F., PRIDMORE-BROWN D.C., 1968, *Dynamics of Mechanical and Electromechanical Systems*, New York: McGraw Hill
4. CUDNEY H.H., BATRA R.C., INMAN D.J., CLAUS R.O., GAUL L., 1999, *Engineering and Designing Smart Structures*, Lecture notes by Virginia Tech.
5. CULSHAW B., 1996, *Smart Structures and Materials*, New York: Artech House
6. FULLER C.R., ELLIOTT S.J., NELSON P.A., 1996, *Active Control of Vibration*, London: Academic Press
7. GANDHI M.V., THOMPSON B.S., 1992, *Smart Materials and Structures*, London: Chapman & Hall
8. HAGOOD N.W., VON FLOTOW A.H., 1991, Damping of structural vibrations with piezoelectric materials and passive electrical networks, *J. Sound and Vibration*, **146**, 2
9. DELL'ISOLA F., HENNEKE E.G., PORFIRI M., 2001, Synthesis of electrical networks interconnecting PZT actuators to damp mechanical vibrations, *Proceedings ISEM, Tokyo 2001, to appear in Journal of Applied Electro-Magnetism and Mechanics*
10. NAYFEH A.H., 1981, *Introduction to Perturbation Techniques*, New York: Wiley Interscience
11. NEAR C.D., 1996, Piezoelectric actuator technology, *SPIE Proceedings: Smart Materials and Structures*, **2715**
12. PERKINS N.C., MOTE C.D., 1986, Comment on curve veering in eigenvalue problems, *J. Sound and Vibration*, **106**, 3

13. RICHARD C., GUYOMAR D., AUDIGIER D., CHING G., 1999, Semi-passive damping using continuous switching of a piezoelectric device, *SPIE Proceeding Passive damping and Isolation*, **3672**, California
14. ROGACHEVA N.N., 1994, *The theory of piezoelectric shells and plates*, Boca Raton: CRC Press
15. SMITH R.C., OUNAIES Z., 1999, A domain wall model for hysteresis in piezoelectric materials, *ICASE Report*, **99-52**
16. UTKU S., 1998, *Theory of Adaptive Structures*, Boca Raton: CRC Press
17. VALIS T., VON FLOTOW A.H., HAGOOD N.W., 1991, An acousto-electromagnetic piezoelectric waveguide-coupler, *SPIE Proceedings: Active Materials and Adaptive Structures*, Virginia
18. VIDOLI S., DELL'ISOLA F., 2000, Modal coupling in one-dimensional electro-mechanical structured continua, *Acta Mechanica*, **141**, 1-2
19. VIDOLI S., DELL'ISOLA F., 2001, Vibration control in plates by uniformly distributed actuators interconnected via electric networks, *European J. of Mechanics A/Solids*, **20**, 435-456
20. VIDOLI S., VESTRONI F., A perturbation approach to veering phenomena, in preparation
21. WOŹNIAK C., 1993, Refined macro-dynamics of periodic structures, *Arch. Mech.*, **45**, 3, 295-304
22. ZELENKA J., 1986, *Piezoelectric Resonators and Their Applications*, Amsterdam: Elsevier

Klasa układów elektromechanicznych: dynamika liniowa i nieliniowa

Streszczenie

W pracy przedstawiono analizę liniowego i nieliniowego zagadnienia dynamiki układów elektromechanicznych, charakteryzujących się wewnętrznym sprzężeniem żyroskopowym. Ze względu na techniczną wartość problemu tłumienia i sterowania drganiami, główny nacisk położono na procesy wymiany energii między podzespołami mechanicznymi i elektrycznymi. W celu zmaksymalizowania przepływu i transformacji energii określono optymalne parametry układu i ich modyfikacje w przypadku nieliniowym.

Manuscript received August 3, 2001; accepted for print December 5, 2001